## Staging of Gastric Carcinoma with Multidetector Computed Tomography

#### Essay

## Submitted for Partial Fulfillment of Master Degree in Radiodiagnosis

Presented by

#### **Waleed Mohammed Mahmood Mohammed**

Resident of Radiodiagnosis Sohag Cancer Institute

Under Supervision of

#### Prof. Dr. Abeer Abd El Maksoud Hafez

Professor of Radiodiagnosis Faculty of Medicine - Ain Shams University

#### Dr. Amir Louis Louka

Lecturer of Radiodiagnosis Faculty of Medicine - Ain Shams University

Faculty of Medicine
Ain Shams University
2011

## **List of Contents**

Title	Page
♦ Introduction and Aim of the Work	1
♦ Chapter 1:	
Anatomical Considerations	4
■ Chapter 2:	
<ul> <li>Normal CT Anatomy of the Stomach</li> </ul>	12
■ Chapter 3:	
Pathological Considerations	19
■ Chapter 4:	
■ Technique of Examination	29
■ Chapter 5:	
<ul> <li>Manifestations and Staging of Gastric Cancer on Multidetector Computed Tomography</li> </ul>	43
♦ Summary and Conclusion	86
♦ References	89
A Arabic Summary	

## **List of Figures**

Fig. No	Title	Page
Figure (1):	The regions of the stomach	5
Figure (2):	Outline of stomach, showing its anatomical landmarks	8
Figure (3):	The arterial supply of the stomach	10
Figure (4):	Lymphatic drainage of the Stomach	11
Figure (5):	Normal gastric wall anatomy as demonstrated using MDCT	12
Figure (6):	Coronal contrast-enhanced multislice CT scan obtained with water as an oral contrast agent demonstrates the normal appearance of the stomach	13
Figure (7):	CT scans of a 72-year-old woman. The stomach is well distended, with water allowing excellent visualization of the enhancing gastric wall with normal folds	14
Figure (8):	A shaded-surface display view accentuates the normal rugal folds of the stomach	14
Figure (9):	A normal stomach	15
Figure (10):	Contrast-enhanced axial multidetector CT image in 65-year-old man without gastric disease shows moderate antral wall thickening (arrowheads) relative to gastric body	16
Figure (11):	Contrast-enhanced axial multidetector CT image in 45-year-old woman without gastric disease shows prominent short-segment circumferential wall thickening (arrowheads) of distal gastric antrum	16

Fig. No	Title Page
Figure (12):	Multidetector computed tomography 3d angiography (3MDCT) imaging; arterial and venous variants were detected by MDCT
Figure (13):	(a) Japanese classification of early gastricic cancer and (b) Borrmann classification of advanced gastric cancer23
Figure (14):	Virtual gastroscopy image shows no abnormal mucosal lesion37
Figure (15):	Sagittal (a) and axial oblique (b) volume rendered CT angiography (CTA) demonstrate the normal anatomy of the celiac axis
Figure (16):	Coronal maximum-intensity projection delineates the normal vasculature around the stomach
Figure (17):	2-dimensional axial CT image shows focal polypoid enhanced lesion in prepyloric antrum
Figure (18):	Coronal (a) and axial oblique (b) contrast-enhanced 3D volume rendered CT scans obtained in a patient with gastric cancer demonstrate focal thickening of the pylorus and distal antrum
Figure (19):	Virtual gastroscopy image shows similar polypoid lesion located in prepyloric antrum44

Fig. No	Title	Page
Figure (20):	Early gastric cancer in 33-year-old woman	45
Figure (21):	Advanced gastric cancer in 62-yearold man	46
Figure (22):	Advanced gastric cancer. Coronal reformatted image shows focal wall thickening in the antrum with marked enhancement of the mucosal layer	46
Figure (23):	Advanced gastric cancer. Sagittal reformatted image shows diffuse thickening of the gastric wall in the fundus and body regions due to linitis plastica	47
Figure (24):	Early gastric cancers. Sagittal reformatted image shows diffuse thickening of the gastric wall in the fundus and body regions due to linitis plastica	48
Figure (25):	(a) Coronal contrast-enhanced 3D volume- rendered CT scan obtained in a patient with gastric cancer demonstrates segmental wall thickening. (b) Axial scan obtained in the same patient reveals invasion of the anterior abdominal wall by the mass	49
Figure (26):	Coronal contrast-enhanced 3D volume- rendered multi-detector row CT scans obtained in a patient with gastric cancer depict the mass	49
Figure (27):	Early gastric cancer (T1) in a 64-year-old woman	53
Figure (28):	Early gastric cancer in a 47-year-old man (T1)	54

Fig. No	Title Pa	ge
Figure (29):	Transverse CT image of a 75-year-old man with tumor in the body of the stomach (arrows) and transmural involvement with linear stranding in the perigastric fat (arrowhead)	5
Figure (30):	Images of a 73-year-old-man5	5
Figure (31):	Intramural gastric carcinoma in a 41- year-old woman (T2)5	6
Figure (32):	Extramural gastric carcinoma in a 51-year-old man (T3)5	7
Figure (33):	Transverse CT scan of a 47-year-old woman shows an antral tumor (arrows) with blurring of more than one-third of the tumor extent (arrowheads)	8
Figure (34):	Images of a 52-year-old woman5	9
Figure (35):	Gastric carcinoma in a 55-year-old woman (T4)6	0
Figure (36):	(a) Coronal reformatted image shows a stage T3 tumor (arrows), with gross infiltration of the perigastric fat tissue in the antrum. (b) Axial CT scan shows a stage T4 tumor with invasion of the colon. The tumor represents an advanced cancer of the antrum and is accompanied by obliteration of the fat plane and thickening of the colonic wall (arrows). (c) Coronal reformatted image shows a stage T4 tumor (arrow) infiltrating the distal pancreatic body. (d) Axial CT scan shows a stage T4 tumor (arrows), an advanced cancer with gross infiltration of the lateral segment of the liver	1

Fig. No	Title	Page
Figure (37):	Advanced gastric cancer (pathologic stage T4)	62
Figure (38):	Three-dimensional volume rendering of gastric carcinoma showing infiltration to the colon	63
Figure (39):	Normal lymph nodes in gastric cancer	65
Figure (40):	Lymph node metastases in gastric cancer (pathologic stages N1-N3)	66
Figure (41):	Multiple hepatic metastases in a 58-year-old man with stomach cancer	68
Figure (42):	Gastric carcinoma with hepatic metastases at segment 6	68
Figure (43):	Krukenberg tumor in a 34-year-old woman with stomach cancer	
Figure (44):	Peritoneal metastasis in a 38-year-old man with stomach cancer	70
Figure (45):	Spread of gastric cancer	71
Figure (46):		72
Figure (47):	Peritoneal metastasis from poorly differentiated adenocarcinoma in a 59-year-old man with stomach cancer	72
Figure (48):	Peritoneal metastasis in a 34-year-old woman with stomach cancer	73
Figure (49):	Contrast-enhanced CT scan obtained with water as an oral contrast agent demonstrates segmental thickening of the stomach (arrows), a finding that represents gastric lymphoma	74
Figure (50):	Contrast-enhanced CT scan obtained with water as an oral contrast agent demonstrates subtle segmental thickening of the gastric antrum (arrow). Endoscopic biopsy revealed gastric lymphoma	74

Fig. No	Title	Page
Figure (51):	Homogeneous wall thickening is a common feature of gastric lymphoma and the most frequently involved site is the distal half of the stomach	75
Figure (52):	Associated lymph node enlargement in lymphoma can be extensive	76
Figure (53):	50-year-old man with low-grade gastric mucosa-associated lymphoid tissue (MALT) lymphoma	77
Figure (54):	Gastric lymphoma	78
Figure (55):	Coronal oblique contrast-enhanced CT scan demonstrates a smooth gastric mass in the antrum	79
Figure (56):	Sagittal (a) and axial oblique (b) contrast-enhanced CT scans demonstrate a round, 5-cm exophytic mass (arrows) that arises from the stomach. The mass proved to be a benign gastrointestinal tumour (GIST) at surgery	80
Figure (57):	Coronal contrast-enhanced CT scan demonstrates a large, ulcerating exophytic mass (arrows) that arises from the stomach, a finding that is compatible with a malignant GIST	80
Figure (58):	Small GISTs are frequently homogeneous in attenuation	81
Figure (59):	Carcinoid tumor	83
Figure (60):	Enhancing metastases to the stomach from malignant melanoma are demonstrated, together with retrocrural and coeliac axis lymph node enlargement and widespread cutaneous deposits	84
Figure (61):	Metastases to the stomach	85

#### **List of Abbreviations**

AGC ······	··Advanced Gastric Cancer
СТ	··Computed Tomography
CTA	··Computed Tomographic Angiography
2D	··Two Dimentional
3D	··Three Dimentional
EGC	··Early Gastric Cancer
EUS	··Endoscopic Ultrasonography
GISTs	··Gastrointestinal Stromal Tumours
MALT	··Mucosa-Associated Lymphoid Tissue
MDCT	··Multi Detector Computed Tomography
MDCTA ······	··Multi Detector Computed Tomography Angiography
MEN	··Multiple Endocrine Neoplasia
MIP	··Maximum Intensity Projection
MPR	··Multi Planner Reconstruction
MSCT	··Multi Slice Computed Tomography
NET	··Neuro Endocrine Tumour
PGC ·····	··Poorly Differentiated Gastric Carcinoma
SSD	··Shaded Surface Display
<b>VP</b>	··Vessel Probe
VR	··Volume Rendering
<b>WGC</b>	··Well Differentiated Gastric Carcinoma

#### Introduction

Throughout the 20<sup>th</sup> century, gastric cancer has been one of the two leading causes of cancer mortality worldwide. In the United States, gastric cancer ranks 14<sup>th</sup> in the number of cancer related mortality (*Kim et al., 2006*).

The majority of patients present with advanced disease and symptoms such as weight loss, vomiting, anorexia, abdominal pain, haematemesis, melaena and pallor (*Alatise et al.*, 2007).

To reduce mortality, it is essential to choose an optimal therapeutic approach, and this in turn depends on early detection and accurate preoperative staging. Early detection is hindered by the relatively non specificity of symptoms in patients with gastric neoplasm (*Kim et al.*, 2006).

Conventional endoscopy is the established primary diagnostic investigation for patients suspected to have gastric malignancy. However, conventional endoscopy has limited value for accurate staging of gastric cancer especially the determination of depth of infiltration, and does not contribute to nodal staging (*Bhandari et al.*, 2007).

In deed, prognosis is related to the depth of invasion of the gastric wall and lymph node involvement (*Chen et al.*, 2007).

With the advent of multidetector computed tomography and endoscopic ultrasound (EUS); the ability to detect, diagnose and characterize disease has improved. These two imaging methods have complementary roles (*Hargunani et al.*, 2007).

Multidetector computed tomography offers new opportunities in imaging of the gastrointestinal tract. When thin collimation is used, near isotropic imaging of the stomach is possible, allowing high quality multiplanar reformation (MPR) and three dimensional (3D) reconstruction of gastric images. Proper distension of the stomach and optimally timed administration of intravenous contrast material are required to detect and characterize disease (*Bas-Salamah et al.*, 2003).

Simple two dimensional multiplanar reformatted images of the CT data allow quick visualization of the stomach in axial, sagittal and coronal planes .It is often helpful to start with two dimensional multiplanar reformations and then proceed to three dimensional volume rendering imaging (*Horton et al.*, 2003).

Multiplanar reconstruction images provide an overall accuracy significantly better than that of transverse images for tumor staging (*Chen et al.*, 2007).

#### Aim of the Work

The aim of the work is to emphasize the role of multidetector computed tomography in staging of gastric cancer.

# Anatomical Considerations Anatomy of the Stomach

The stomach is the most dilated organ of the body. It lies in the epigastric, umbilical, and left hypochondrial areas of the abdomen (*Healy*, 2005).

It is J-Shaped but varies in size and shape with the volume of its contents, with erect and supine position, and even with inspiration and expiration (*Ryan et al.*, 1994).

The stomach was anatomically divided into the proximal portion (fundus), the middle portion (body), the distal portion (antrum) and the most distal portion (pylorus) (*Fielding and Hallissey*, 2005).

The stomach has two orifices, the cardiac orifice at esophago-gastric junction and the pyloric orifice. It has two curvatures, the greater curvature and lesser curvature. The incisura is an angulation of the lesser curve. The part of the stomach above the cardia is called the fundus. Between the cardia and incisura is the body of the stomach and distal to the incisura is the antrum .The cardiac orifice and fundus are relatively excursion of the diaphragm (Fig.1) (Cunningham and Romanes, 1986).

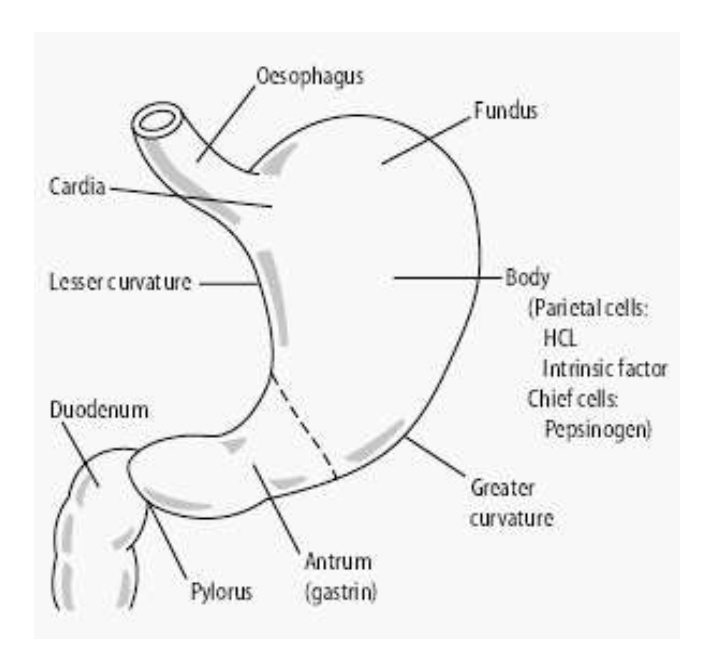


Figure (1): The regions of the stomach (Fielding and Hallissey, 2005).

#### **Gastric Orifices:**

The opening from the esophagus into the stomach is the cardiac orifice situated to the left of the midline behind the seventh costal cartilage. The part of the stomach above the level of the cardiac orifice is the fundus. The pyloric orifice, the opening into the duodenum, is usually indicated by a circular pyloric constriction of the surface of the organ, indicating the pyloric sphincter (*Healy*, 2005).

The stomach wall, like the wall of most other parts of the digestive canal, consists of three layers: the mucosal (the innermost), the muscularis and the serosal (the outermost). The

mucosal layer itself can be divided into three layers: the mucosa (the epithelial lining of the gastric cavity), the muscularis mucosa (low density smooth muscle cells) and the submucosal layer (consisting of connective tissue interlaced with plexi of the enteric nervous system). The second gastric layer, the muscularis, can also be divided into three layers: the longitudinal (the most superficial), the circular and the oblique (Fig.2). The longitudinal layer of the muscularis can be separated into two different categories: a longitudinal layer that is common with the esophagus and ends in the corpus, and a longitudinal layer that originates in the corpus and spreads into the duodenum (Gopu et al., 2008).

#### **Gastric Curvatures:** (Fig.2)

The lesser curvature extends between the cardiac and pyloric orifices. The lesser omentum is attached to the lesser curvature and contains the right and left gastric vessels adjacent to the line of the curvature (*Healy*, 2005).

The greater curvature is directed anteroinferiorly and is four or five times as long as the lesser curvature. It starts from the cardiac incisura and arches upwards, posterolaterally, and to the left. Its highest convexity is at the funds then it turns right to end at the pylorus (*Healy 2005*).